Energy transfer of the Gross-Pitaevskii turbulence in weak-wave-turbulence and strong-turbulence ranges

Kyo Yoshida[1*], Hideaki Miura[2] and Yoshiyuki Tsuji[3]

[1*]Faculty of Pure and Applied Sciences, University of Tsukuba, 1-1-1 Tennoudai, Tsukuba, 305-8571, Ibaraki, Japan.
[2]Department of Helical Plasma Reserarch, National Institute for Fusion Science, 322-6 Oroshi-cho, Toki, 509-5292, Gifu, Japan.
[3]Department of Energy Science and Engineering, Nagoya University, Furo-sho, Chikusa, Naoyga, 464-8601, Aichi, Japan.

*Corresponding author(s). E-mail(s): yoshida.kyo.fu@u.tsukuba.ac.jp;

Abstract

Numerical simulations of quantum fluid turbulence obeying the Gross-Pitaevskii equation are performed with the simulation sizes as large as the weak-wave-turbulence and the strong-turbulence wavenumber ranges coexist in one simulation. The energy cascade is observed within the simulated wavenumber range. The spectrum $\boldsymbol{F(k)}$ in the weak-wave-turbulence range agrees with the $\boldsymbol{k^{-1}}$ scaling without logarithmic correction suggested by a closure approximation (Yoshida and Arimitsu in J Phys A Math Theor 46(33):335501, 2013) and the slope of $\boldsymbol{F(k)}$ in the strong-turbulence range is steeper than that suggested in the same closure approximation. The energy flow from the interaction energy to the kinetic energy during the cascade is also observed.

Keywords: Quantum fluid, Turbulence, Bose-Einstein condensate, Gross-Pitaevskii equation

1 Introduction

Quantum fluids such as Bose-Einstein condensates (BECs) of ultracold atoms and the superfluid component in the superfluid phase of ^{4}He may become turbulence when they are accompanied by external pumping and dissipation. There have been many experimental and numerical studies on the turbulence of quantum fluids. See, e.g., the reviews Refs. [1, 2] and the references cited therein.

The dynamics of quantum fluids are approximately described by the Gross-Pitaevskii (GP) equation , which is a partial differential equation of the order parameter field $\psi(\mathbf{x}, t)(\in \mathbb{C})$, under certain conditions[3–5]. Then, the GP equation equipped with external pumping and dissipation may be one of the models to analyze the turbulence of quantum fluids. The spectrum $F(k)$, where k is the wavenumber, is the basic quantity of interest. The definition of $F(k)$ will be given later in Eq.(3). There is a typical wavenumber k_* in the GP turbulence and the whole wavenumber range may be divided into two ranges, the weak wave turbulence (WWT) range, $k > k_*$, and the strong turbulence (ST) range, $k < k_*$.

In the WWT range, the contribution of the nonlinear term in the GP equation is small and the WWT theory[6, 7] can be used. Dyachenko, Newell, Pushkarev, and Zakharov[8] (hereafter, referred to as DNPZ) applied the WWT theory to the GP turbulence and obtained $F(k) \propto k^{-1}(\ln(k/k_\mathrm{b}))^{-1/3}$ for the energy cascade range, where k_b is the bottom wavenumber of the cascade range, and $F(k) \propto k^{-1/3}$ for the particle-number cascade range.

Yoshida and Arimitsu[9] (hereafter, referred to as YA) analyzed the both WWT and ST range using a closure approximation. Naturally, they obtained the same results as DNPZ for the WWT range with an addition of $F(k) \propto k^{-1}$ without logarithmic correction under the situation that there is a sufficient amount of $F(k)$ in $k < k_\mathrm{b}$. Regarding the ST range, YA obtained $F(k) \propto k^{-2}$ for the energy cascade range and $F(k) \propto k^{-1}$ with a possible logarithmic correction for the particle-number cascade range. It should be noted that the closure approximations are, in general, empirical methods to analyze the system with strong nonlinearity and that they are not mathematically rigorous. (See Ref.[10] for a comprehensive review of the closure approximations in turbulence.) Furthermore, the existence of the energy or particle cascade is an assumption to obtain $F(k)$ both in the WWT theory and the closure approximation and the detailed condition for the emergence of the cascades is not evident. Therefore, $F(k)$ obtained from DNPZ or YA should be verified by numerical simulations or experiments.

The GP turbulence has been numerically studied from many aspects. See, e.g., Refs. [11–13]. Some studies are more oriented to the analysis of the velocity field, $\mathbf{v} = \nabla\theta$ with $\psi = \sqrt{\rho}\mathrm{e}^{\mathrm{i}\theta}$, rather than the order parameter field ψ itself, or to analysis some finite temperature effects. Here, we are focusing on the statistics of ψ at the zero-temperature limit with minimum pumping and dissipation. The numerical study most relevant to the present study is that by Proment, Nazarenko, and Onorato[14] (hereafter, referred to as PNO). They

performed numerical simulations of GP turbulence to obtain both $F(k) \propto k^{-1}$ and $F(k) \propto k^{-2}$ by changing the parameter ξ. They may correspond to the energy cascade range of WWT and ST. The particle cascade with $F(k)$ consistent with YA is observed in the numerical simulation for far ST range $k \ll k_*$[15]. Despite these studies, it may be said that a comprehensive understanding of the spectrum $F(k)$ of the GP turbulence has not been achieved yet.

To add to the understanding, we performed the numerical simulations of GP turbulence focusing on the connection between the WWT range and the ST range around the wavenumber k_*. Although the WWT and ST ranges were simulated in NPO, the size of the simulations was limited so that the two ranges are realized separately in different simulations. We set the size of the numerical simulations to be so large that both WWT in the wavenumber range $k > k_*$ and ST in the wavenumber range $k < k_*$ exist in one simulation. We are especially interested in the energy transfer in the wavespace as well as the spectrum $F(k)$.

2 Set up of Numerical Simulations

We performed simulations of the GP equation with external pumping and dissipation of the mass. Regarding the basic setting, we follow those of Ref. [15, 16]. The domain of the fluid is a three-dimensional cube with the side length 2π and the periodic boundary condition is applied to each direction of the sides. Hence, the wavevector is discretized with the unit $\Delta k = 1$ in each direction.

The GP equation in wavevector space is given by

$$\frac{\partial}{\partial t}\psi_{\mathbf{k}} = -\mathrm{i}\xi^2 k^2 \psi_{\mathbf{k}} + \mathrm{i}\psi_{\mathbf{k}} - \mathrm{i} \sum_{\mathbf{k}+\mathbf{p}-\mathbf{q}-\mathbf{r}=\mathbf{0}} \psi^*_{\mathbf{p}} \psi_{\mathbf{q}} \psi_{\mathbf{r}} + D_{\mathbf{k}} + P_{\mathbf{k}}, \tag{1}$$

where $k = |\mathbf{k}|$, $\psi_{\mathbf{k}}(t)$ (the time index t is omitted) is the Fourier transform of the order parameter field $\psi(\mathbf{x}, t) \in \mathbb{C}$, $\xi := \hbar/\sqrt{2mg\overline{n}}$ is the healing length, m is the mass of the particle, $g(> 0)$ is the coupling constant, $\overline{n}$ is the average particle number density, $D_{\mathbf{k}}$ and $P_{\mathbf{k}}$ represent the dissipation and pumping of mass, respectively, the chemical potential is set to $\mu = g\overline{n}$, and the unit system such that $\hbar = g = \overline{n} = 1$ is used. An alias-free spectral method is used for the cubic term in ψ so that the maximum resolved wavenumber $k_{\max}$ is $N/4$ where N is the number of grid points along each direction. A fourth-order Runge-Kutta method is used for the time evolution.

We apply dissipation and pumping mainly acting on large and small wavenumber modes, respectively, in order to investigate the general property of energy transfer in the inertial range that locates in the intermediate range. Expecting that the details of dissipation and pumping have little effect on the inertial range when the dissipation and pumping wavenumber ranges are well

Table 1 Parameters in the simulations.

	ξ	ν_4	γ	$k_{\rm p}$	N	$k_{\rm max}$	Δt	$\epsilon_{\rm K}$
RUN1	0.064	0.25×10^{-13}	1.0	2.5	1024	256	0.00125	0.000031
RUN2	0.032	0.32×10^{-11}	4.0	2.5	1024	256	0.005	0.0024
RUN3	0.016	0.125×10^{-10}	4.0	2.5	1024	256	0.01	0.0017

ξ: the healing length, ν: the coefficient of the dissipation term, $k_{\rm p}$: the top wavenumber of the pumping range, N: number of grid points along a coordinate direction, $k_{\rm max}$: maximum wavenumber resolved, Δt: the time increment, $\epsilon_{\rm K}$: kinetic energy dissipation rate at the final state of the simulation. All the values are given in the unit system such that $\hbar = g = \overline{n} = 1$ and $\Delta k = 1$.

separated, we employ simple models of dissipation and pumping as

$$D_{\mathbf{k}} = -\nu_4 k^\ell \psi_{\mathbf{k}} - \gamma \delta_{\mathbf{k},\mathbf{0}}, \qquad P_{\mathbf{k}} = \begin{cases} \alpha \psi_{\mathbf{k}} & (0 < k \le k_{\rm p}) \\ 0 & \text{otherwise} \end{cases}. \tag{2}$$

Here, $\ell = 4$, $\nu_4, \gamma, k_{\rm d} > 0$ and $\delta_{\mathbf{k},\mathbf{k}'}$ is the Kronecker delta. The value of ℓ is replaced from $\ell = 2$ in the previous work [15] in order to confine the dissipation in a narrower range and to broaden the inertial range. An additional damping is applied to the mode $\mathbf{k} = \mathbf{0}$ in order to avoid the uniform accumulation of the mass. The parameter α is determined at every time step so that $\overline{n} = 1$ is almost satisfied.

The parameters of the simulations are summarized in Table 1. In the present study, we aim to realize two wavenumber range, that is, the WWT range ($k > k_*$) and the ST range ($k < k_*$) in one simulation, where $k_* := \xi^{-1}$. To this end, the number of grid points along a coordinate direction is set to as large as $N = 1024$. The pumping of the mass is located in the wavenumber range $k \le k_{\rm p} = 2.5$ and ν_4 is so chosen that the dissipation mainly acts in the large wavenumber range $k > 100$. We set $\xi = 0.064, 0.032$ and 0.016 so that $k_* = 15.625, 31.25$ and 62.5, respectively, are located between the pumping and dissipation wavenumber ranges.

In general, the energy transfer due to nonlinear interactions is suppressed for large ξ and excitation of large wavenumber modes are suppressed for large ν_4. We first performed preliminary simulations with some small ξ and large ν_4 to obtain a developed state within a small wavenumber range efficiently. Then ξ was increased and ν_4 was decreased gradually to those values given in Table 1. No less than 7×10^5 time steps are computed after the values of ξ and ν_4 reached those in Table 1 in order to obtain a statistically quasi-stationary state. At a statistically quasi-stationary state, the energy balance relation $\Pi(k) \approx \epsilon$ should be satisfied for k in the inertial range where $\Pi(k)$ is the total energy flux through the wavenumber k and ϵ is the total energy dissipation. As we will see in Sec.4, the most of the energy dissipation rate ϵ is the kinetic energy dissipation rate $\epsilon_{\rm K}$. The value of $\epsilon_{\rm K}$ at the final state of RUNs are also given in Table 1. The explicit definition of $\Pi(k)$ and $\epsilon_{\rm K}$ will

be given later in Sec. 3. The energy balance relation was not achieved within the simulated time interval of RUN1. This is because the typical time scale of the energy transfer in the WWT range scales as $\propto k^2$ and the time evolution of $F(k)$ in the deep WWT range $k \gg k_*$ is so slow that the sytem has not reached a quasi-stationary state within the simulated time period. Therefore, we mainly analyze the quasi-stationary states obtained in RUN2 and RUN3 in the following.

3 Spectrum and Flux

The spectrum $F(k)$ in the present simulations is defined by

$$F(k) := \sum_{\mathbf{k}' \in \mathrm{Sh}(k)} |\psi_{\mathbf{k}'}|^2, \tag{3}$$

where $\mathrm{Sh}(k) = \{\mathbf{k}' | k - 1/2 \le k' < k + 1/2\}$. The kinetic energy E_K and the interaction energy E_I are given by

$$E_\mathrm{K} := \sum_{\mathbf{k}} \xi^2 k^2 |\psi_{\mathbf{k}}|^2, \quad E_\mathrm{I} := \frac{g}{2} \sum_{\mathbf{k},\mathbf{p},\mathbf{q},\mathbf{r}} \delta_{\mathbf{k}+\mathbf{p}-\mathbf{q}-\mathbf{r},\mathbf{0}} \psi^*_{\mathbf{k}} \psi^*_{\mathbf{p}} \psi_{\mathbf{q}} \psi_{\mathbf{r}} = \frac{g}{2} \sum_{\mathbf{k}} |n_{\mathbf{k}}|^2, \tag{4}$$

where $n_{\mathbf{k}}$ is the Fourier transform of the particle number field $n(x) = |\psi(x)|^2$. Since the interaction energy is a summation of the fourth-order moments $\psi^*_{\mathbf{k}} \psi^*_{\mathbf{p}} \psi_{\mathbf{q}} \psi_{\mathbf{r}}$ involving various wavevector modes $\mathbf{k}, \mathbf{p}, \mathbf{q}$, and $\mathbf{r}$, the definiton of the interaction energy density in wavevector space is not unique. However, note that the interaction energy may be written as a summation of second order terms in $n_{\mathbf{k}}$. Here, we choose to define the interaction energy density at $\mathbf{k}$ by using $n_{\mathbf{k}}$, that is, $(g/2)|n_{\mathbf{k}}|^2$. Note that the total energy $E = E_\mathrm{K} + E_\mathrm{I}$ is conserved by the nonlinear interactions.

The kinetic and interaction energy transfers at wavenumber k can be defined as

$$T_\mathrm{K}(k) := \sum_{\mathbf{k}' \in \mathrm{Sh}(k)} \xi^2 k'^2 \left. \frac{\partial}{\partial t} \right|_{D,P=0} |\psi_{\mathbf{k}'}|^2, \quad T_\mathrm{I}(k) := \sum_{\mathbf{k}' \in \mathrm{Sh}(k)} \frac{g}{2} \left. \frac{\partial}{\partial t} \right|_{D,P=0} |n_{\mathbf{k}'}|^2, \tag{5}$$

where $(\partial/\partial t)|_{D,P=0}$ denotes the time derivative without dissipation and pumping. The total energy flux

$$\Pi(k) := \sum_{k' \ge k} \left(T_\mathrm{E}(k') + T_\mathrm{I}(k') \right) = - \sum_{k' < k} \left(T_\mathrm{E}(k') + T_\mathrm{I}(k') \right), \tag{6}$$

is the total energy flowing from the modes with wavenumber smaller than $k - 1/2$ to the modes with wavenumber equal or larger than $k - 1/2$ per unit time.

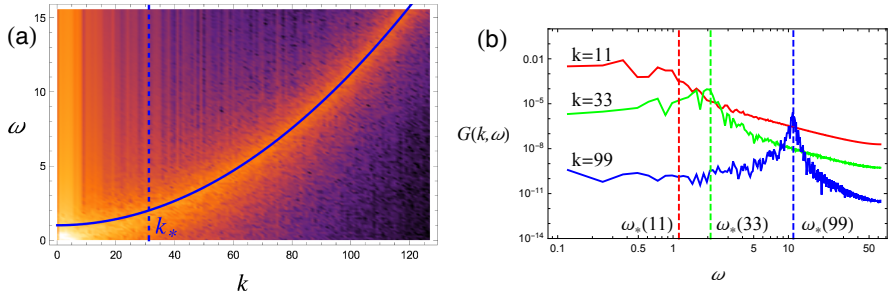

Fig. 1 (a) The density plot of the frequency spectrum $G(k,\omega)$ of $\mathbf{k} = (\pm k, 0, 0)$ (averaged over $\pm k$) for RUN2 ($k_* = 31.25$). The bright region corresponds to large $G(k,\omega)$ and the brightness scales logarithmically with $G(k,\omega)$. Solid line indicates the dispersion relation $\omega_*(k) = \xi^2 k^2 + 1$. (b) The same frequency spectrum $G(k,\omega)$ for fixed wavenumbers $k = 11(< k_*)$, $k = 33(\sim k_*)$ and $k = 99(> k_*)$ in solid lines. The dashed lines indicate $\omega_*(k)$.

The kinetic energy dissipation rate $\epsilon_{\rm K}$ is given by

$$\epsilon_{\rm K} = \sum_{\mathbf{k}} \nu_4 \xi^2 k^{2+\ell} |\psi_{\mathbf{k}}|^2. \tag{7}$$

4 Results of the simulations

Before the analysis of the spectrum $F(k)$ and the flux $\Pi(k)$, we first verify the frequency spectrum $G(\mathbf{k},\omega) = |\phi_{\mathbf{k}}(\omega)|^2$ where $\phi_{\mathbf{k}}(\omega)$ is the Fourier transform of $\psi_{\mathbf{k}}(t)$ with respect to t. For the Fourier transform, 1024 time-series data of $\psi_{\mathbf{k}}(t)$ were taken at the time interval $10\Delta t$ after $F(k)$ reached quasi-stationary states in RUN2 and RUN3, where Δt is the time increment of the simulation. For saving the computational resources, we computed $G(\mathbf{k},\omega)$ only for the wavevector modes on the x-axis, that is, $\mathbf{k} = (k, 0, 0)$. The obtained frequency spectrum $G(\mathbf{k},\omega)$ is given in Fig.1 for RUN2. Figures for RUN3 are omitted.

In the wavenumber region $k > k_*$, an apparent peak of $G(\mathbf{k},\omega)$ along the dispersion relation $\omega_*(k) = \xi^2 k^2 + 1$ is observed. The sharp peak indicates that the effects of the nonlinearity and the dissipation are small in the region. The width of the peak broadens in the wavenumber region $k < k_*$. This implies that the nonlinearity dominates over the linear wave motion in the wavenumber region. Thus, we confirmed that the frequency spectrum $G(\mathbf{k},\omega)$ is consistent with the picture that $k > k_*$ is the weak wave turbulence range and that $k < k_*$ is the strong turbulence range.

The kinetic and interaction energy transfers $T_{\rm K}(k)$ and $T_{\rm I}(k)$, respectively, and the total energy flux $\Pi(k)$ of the quasi-stationary states in RUN2, RUN3 are given in Figs.2 (a) and (b). They are the averages over 81 snapshots at the time interval $5,000\Delta t$. We observe a negative peak of $T_{\rm I}(k)$ in a small-wavenumber region and a positive peak of $T_{\rm K}(k)$ in a large-wavenumber region in both RUN2 and RUN3. These imply that the interaction energy in the small-wavenumber region is transferred to the kinetic energy in the large-wavenumber region by the nonlinear interactions as a whole. Since the

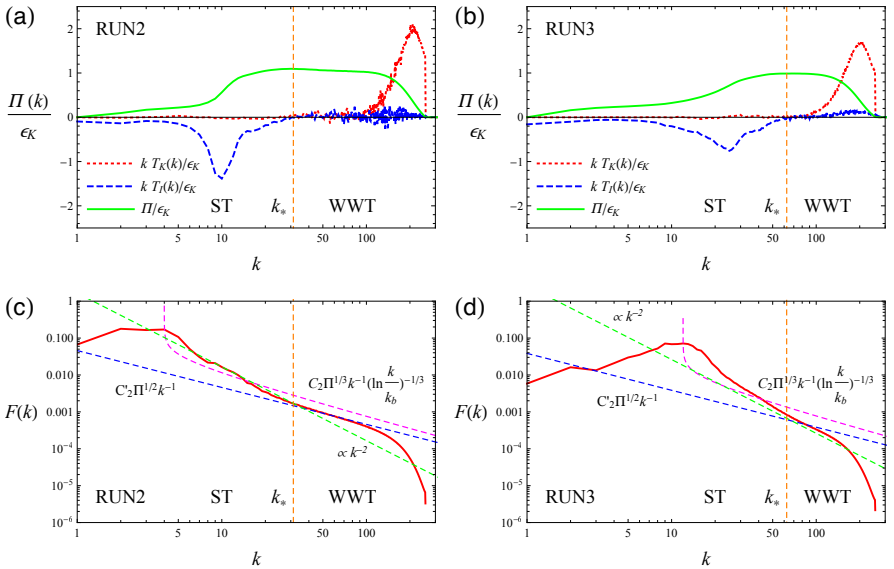

Fig. 2 The kinetic energy transfer $T_K(k)$, interaction energy transfer $T_I(k)$, total energy flux $\Pi(k)$ and spectrum $F(k)$ in RUN2($\xi = 0.032$) and RUN3($\xi = 0.016$). The wavenumber $k_*(= \xi^{-1})$ indicates the boundary between the weak wave turbulence (WWT) range and the strong turbulence (ST) range. Spectra suggested in Ref.[9] , $C_2\Pi^{1/3}k^{-1}(\ln(k/k_b))^{-1/3}$, $C_2'\Pi^{1/2}k^{-1}$ for WWT range and $\propto k^{-2}$ for ST range, are plotted in dashed lines together with $F(k)$ of RUN2 and RUN3. The kinetic energy dissipation rate ϵ_K is used for the normalization of the transfers and flux.

statistical quasi-stationarity is attained, the energy is externally supplied in the small wavenumber region in the form of the interaction energy and the kinetic energy in the large-wavenumber region is dissipated by the hyper-viscosity. Absence of a negative peak of $T_K(k)$ and a positive peak of $T_I(k)$ suggest that there are little external injection of kinetic energy and little dissipation of interaction energy, respectively. Let k_{in} be the negative peak wavenumber of $T_I(k)$ and k_{dis} be the positive peak wavenumber of $T_{K(k)}$ Then, we have $\epsilon_I^{(in)} \approx \Pi(k) \approx \epsilon_K$ for $k_{in} \lesssim k \lesssim k_{dis}$ and $\epsilon_K^{(in)} \approx \epsilon_I \approx 0$, where $\epsilon_K^{(in)}$ and $\epsilon_I^{(in)}$ are the kinetic and ineteraction energy injection rates, respectively, ϵ_K and ϵ_I are the kinetic and interaction energy dissipation rates, respectively. Since the interaction energy around k_{in} is transferred to the kinetic energy around k_{dis}, the energy must be transformed from the interaction energy to the kinetic energy during the energy cascade process from k_{in} to k_{dis}.

We can see in Fig. 2(a) that the constant total energy flux $\Pi(k) \approx \epsilon_K$, where ϵ_K is the kinetic energy dissipation rate, is approximately satisfied in a wavenumber range around $10 < k < 100$ of RUN2. Since $k_* = 31.25$ is the typical wavenumber that separates the WWT range and the ST range, we may consider $k_* < k < 100$ to be the energy cascade range of WWT and $10 < k < k_*$ to be that of ST.

Although the external pumping of mass is applied in a wavenumber range $0 < k \leq k_p = 2.5$, the external injection of interaction energy is located at

larger wavenumbers around $k_{\rm in}$. This may happen since $n_{\mathbf{k}}$ is nonlinear in $\psi_{\mathbf{k}}$ and an external excitation of $\psi_{\mathbf{k}}$ has an effect on $n_{\mathbf{k}'}$ with $\mathbf{k}' \neq \mathbf{k}$. Moreover, the wavenumber $k_{\rm in}$ increases with k_* so that the energy transfer range do not broaden far into the ST range $k \ll k_*$ in RUN3. See Fig. 2(b).

It is pointed out in YA that there can be two types of spectrum $F(k)$ for the energy cascade range of WWT, that is,

$$F(k) = C_2 \Pi^{1/3} k^{-1} \left(\ln \frac{k}{k_{\rm b}} \right)^{-\frac{1}{3}} \quad \text{and} \quad F(k) = C_2' \Pi^{1/2} k^{-1}, \tag{8}$$

in the present unit system, where $k_{\rm b}$ is the bottom wavenumber of the scaling range, $C_2 = (4\pi^4 (3/2) I_2)^{-1/3}$ and $C_2' = I_2^{-1/2}/2\pi^2$ with $I_2 \simeq 0.00298$. (The factor (3/2) is missing in YA.) The former is identical to the one given in DNPZ. The former(latter) form is for the case that the amplitude of $F(k)$ is small(large) in the range $k < k_{\rm b}$. Two types of spectrum $F(k)$, Eq.(8), are also plotted in Figs. 2(c) and (d), where $k_{\rm b}$ is set to the peak wavenumber of $F(k)$. The spectrum $F(k)$ of RUN2 agrees with the latter spectrum rather than the former in the energy cascade range of WWT. Although the scaling range is quite narrow, the agreement is not only for the scaling k^{-1} but also up to the constant C_2'. Since a considerable amount of $F(k)$ is present in $k < k_*$, the agreement with the latter spectrum in (8) is plausible. By letting k_* to a smaller value, we may broaden the WWT range. RUN1 corresponds to such parametrization and the k^{-1}-scaling range broadens indeed. However, since the statistical stationarity is not achieved in RUN1, we omit to show the figure and the qualitative analysis. Conversely, the WWT range shrinks and the k^{-1}-scaling is hardly observed in RUN3.

It is suggested in YA that

$$F(k) = C_1 \xi^{-1/2} \Pi^{1/2} k^{-2}, \tag{9}$$

where the constant C_1 is not fixed, in the energy transfer range of ST. The slope of $F(k)$ in the ST range is steeper than that in the WWT range for both RUN2 and RUN3. Regarding RUN2, the slope of $F(k)$ seems to be consistent with k^{-2} in the energy cascade range of the ST. However, the verification of (9) is not definitive since the scaling range is quite narrow and C_1 is not determined from the theory. The value of $C_1 \approx 6$ may be a possible estimate from RUN2. The dashed line with slope $\propto k^{-2}$ in Fig. 2 (c) corresponds to $C_1 = 6$. Despite the ST range being broader in RUN3 than in RUN2, the energy cascade range, where the total energy flux is approximately constant, within the ST range do not broaden so much in RUN3. Furthermore, the slope of $F(k)$ seems to be steeper that k^{-2} in this narrow range.

5 Discussion

In the present simulations, both WWT and ST ranges are realized in one simulation by taking a sufficient simulation size (1024^3 grid points) and setting parameters, especially ξ, to suitable values. In previous studies (e.g., Ref. [14]), the WWT and ST ranges were simulated separately in simulations with a smaller size. To our best knowledge, the clear change of the slope of $F(k)$ around $k_* = \xi^{-1}$ is observed for the first time in the present simulations.

Although two types of spectrum, Eq.(8), for WWT are theoretically suggested, that the distinction between the two spectra in numerical simulations is difficult since a wide scaling range is required to verify the logarithmic correction in general. In the present study, we noticed not only the scaling of $F(k)$ but also the coefficients C_2 and C_2' to analyze the data from numerical simulations. It is confirmed that $F(k) \propto k^{-1}$ without logarithmic correction emerges under the condition that the WWT and ST ranges coexist.

It is difficult to derive a definite conclusion on the scaling of the spectrum $F(k)$ in the energy cascade range of ST from the present numerical simulations. The main reason for the difficulty comes from the narrowness of the energy cascade range in ST. The scaling $F(k) \propto k^{-2}$ in YA is based on the assumption that there is a broad energy cascade range and the assumption is not fulfilled in the simulations. It is not clear whether the narrowness of the energy cascade range is a universal feature or it is due to the specific form of the pumping $P_{\mathbf{k}}$ in Eq. (2). The numerical simulations with a different type of pumping are ongoing and the results would be reported elsewhere.

It is suggested in YA that there is an energy flow from the interaction energy to the kinetic energy in the ST range. The results from the present simulations are consistent with the suggestion. If the energy flow is strong in the deep ST wavenumber range $k \ll k_*$, it may violate the stationary of the spectrum $F(k) \propto k^{-2}$, modify the form of $F(k)$ and weaken the energy cascade process. This is a possible reason of the spectrum $F(k)$ in the ST range of RUN3 is steeper than k^{-2}-scaling and the energy transfer is somewhat suppressed in ST in the sense that the energy transfer range does not broaden with the increase of k_*. It is a future study to analyze these results in terms of the closure approximation developed in YA.

The wavenumber range of the present simulation, that is, the wavenumber range around k_* is relevant to the experimental studies of BEC turbulence (e.g., Refs. [17, 18]). However, the settings of the pumping, dissipation, and boundary conditions in those experiments are different from the present simulation. Therefore, the comparison between the present simulations and those experiments is not straightforward. The detailed discussion on the comparison may be left for a future study.

Acknowledgments. This work was performed on "Plasma Simulator" (FUJITSU FX100, NEC SX-Aurora TSUBASA) of NIFS with the support and under the auspices of the NIFS Collaboration Research program (NIFS18KNSS106, NIFS20KNSS144).

Declarations

The datasets generated during and/or analysed during the current study are available from the corresponding author on reasonable request.

References

[1] Barehnghi, C.F., Skrbek, L., Sreenivasan, K.R.: Introduction to quantum turbulence. Proceedings of the National Academy of Sciences of the United States of America **111**, 4647–4652 (2014)

[2] Tsubota, M., Fujimoto, K., Yui, S.: Numerical studies of quantum turbulence. Journal of Low Temperature Physics **188**, 119–189 (2017)

[3] Pitaevskii, L.P.: Vortex lines in an imperferct Bose gas. Soviet Phys. JETP **13**, 451–454 (1961)

[4] Gross, E.P.: Hydrodynamics of superfluid condensate. J. Math. Phys. **4**, 195–207 (1963)

[5] Pitaevskii, L., Stringari, S.: Bose-Einstain Condensation. Oxford University Press(2003)

[6] Zakharov, V.E., L'vov, V.S., Falkovich, G.: Kolmogorov Spectra of Turbulence I: Wave Turbulence. Springer(1992)

[7] Nazareko, S.: Wave Turbulence. Lecture Notes in Physics, vol. 825. Springer(2011)

[8] Dyachenko, S., Newell, A.C., Pushkarev, A., Zakharov, V.E.: Optical turbulence: weak turbulence, condensates and collapsing filaments in the nonlinear Schrödinger equation. Physica D **57**, 96–160 (1992)

[9] Yoshida, K., Arimitsu, T.: Inertial-range structure of GrossPitaevskii turbulence within a spectral closure approximation. Journal of Physics A:Mathematical and Theoretical **46**(33), 335501 (2013)

[10] Zhou, Y.: Turbulence theories and statistical closure approaches. Physics Reports **935**, 1–117 (2021). https://doi.org/10.1016/j.physrep.2021.07.

001. Turbulence theories and statistical closure approaches

[11] Nore, C., Abid, M., Brachet, M.E.: Decaying Kolmogorov turbulence in a model of superflow. Phys. Fluids **9**, 2644–2669 (1997)

[12] Kobayashi, M., Tsubota, M.: Kolmogorov spectrum of quantum turbulence. J. Phys. Soc. Jpn. **74**, 3248–3258 (2005)

[13] Krstulovic, G., Brachet, M.: Energy cascade with small-scale thermalization, counterflow metastability, and anomalous velocity rings in fourier-truncated gross-pitaveskii equation. Physical Review E **83**, 066311 (2011)

[14] Proment, D., Nazarenko, S., Onorato, M.: Quantum turbulence cascades in the gross-pitaevskii model. Phys. Rev. A **80**, 051603 (2009)

[15] Yoshida, K., Miura, H., Tsuji, Y.: Specturm in the storing turbulence region of Gross-Pitaevskii turbulence. J. Low Temp. Phys. **196(1-2)**, 211–217 (2019)

[16] Yoshida, K., Arimitsu, T.: Energy spectra in quantum fluid turbulence. J. Low Temp. Phys. **145(1-4)**, 219–230 (2006)

[17] Tsatsos, M.C., Tavares, P.E.S., Cidrim, A., Fritsch, A.R., Caracanhas, M.A., dos Santos, F.E.A., Barenghi, C.F., Bagnato, V.S.: Quantum turbulence in trapped atomic boseeinstein condensates. Physics Reports **622**, 1–52 (2016). https://doi.org/10.1016/j.physrep.2016.02.003. Quantum turbulence in trapped atomic BoseEinstein condensates

[18] Navon, N., Gaunt, A.L., Smith, R.P., Hadzibabic, Z.: Emergence of a turbulent cascade in a quantum gas. Nature **539**, 72–75 (2016)